IEEE Access
Multidisciplinary | Rapid Review | Open Access Journal

Received January 25, 2020, accepted March 5, 2020, date of publication March 17, 2020, date of current version March 26, 2020.

Digital Object Identifier 10.1109/ACCESS.2020.2981342

Modeling and Characterization of Series Connected Hybrid Transformers for Low-Profile Power Converters

M. ABU BAKAR, M. FARHAN ALAM, AND KENT BERTILSSON
Department of Electronics Design, Mid Sweden University, 85170 Sundsvall, Sweden
Corresponding author: M. Abu Bakar (MuhammadAbu.Bakar@miun.se)

ABSTRACT Compact and low profile power converters are the main business of today's power industry. A significant volume of a power converter is occupied by the power transformer. This article proposes a unique solution that would make the power converters low profile. Instead of designing a power converter by using a single bulky transformer, the solution proposed is to split the main bulky transformer into a number of low profile transformers. This not only reduces the total weight and volume of the converter but also the total transformer losses. The use of more than one transformer in series reduces the applied voltage on the transformers, which minimizes the required turns ratio and decreases the stress on the secondary rectifiers and filter elements. Moreover, the decrease in the applied voltage reduces the proportional loss per transformer and makes it possible to design a hybrid transformer by combining Litz wire and traces of a printed circuit board. The reduced copper loss and lower heat dissipation per transformer simplify thermal management. An analytical comparison is made between the utilization of a single transformer or a number of transformers. The procedure of splitting a volume of a single transformer into a number of small transformers has been comprehensively discussed. The idea is investigated both experimentally and in computer simulation for an example application of a phase shifted full bridge dc-dc converter. The converter is characterized up to a load power of 2.2 kW at $V_{in} = 400\ \mathrm{V_{dc}}$ and $\mathrm{V}_{out} = 48\ \mathrm{V_{dc}}$.To make the approach more practical, the transformers are modeled using the traditional analytical method. The design of the example application using the split transformer approach reduces the total transformer weight by 45%, compared to the traditional approach with a single transformer. The converter also shows good performance with a maximum efficiency of 96%.

INDEX TERMS Series transformers, modeling of transformers, transformer design, isolated converter, medium power converter, low profile converter, ZVS converter, PSFB converter, lightweight converter.

I. INTRODUCTION

The demand for smarter and low profile electronic solutions is rapidly increasing in nearly all industrial applications. To meet this challenge, the power electronics industry is progressing towards smart and low profile power converters. It ranges from tiny mobile charging applications to high power electric vehicles and smart grid applications [1], [2]. The power density of a power converter has a direct relationship with the switching frequency; increasing the switching frequency has been trending as a way to reach the goal of a compact power converter. The increase in switching frequency reduces the size of the magnetics and the capacitors. However, the increase in switching frequency degrades remaining elements such as switching losses, parasitic effects, proximity losses and electromagnetic noise (EMI). This becomes worse with the increment in power and line voltage. Thus, the increase in switching frequency makes it less favorable [3], [4] for medium and high power applications.

In medium and high power applications, the power transformer occupies a significant volume. This is a main constraint preventing from the improvement of the power density of the converters. As the power level increases, the size and weight of the transformer make it even more difficult to obtain high power density and better efficiency. The loss in power transformers is mainly depends on the applied voltage and switching frequency. The loss increases with the increase in applied volt-second. For fixed frequency power converters, this can be brought down by decreasing the applied voltage

The associate editor coordinating the review of this manuscript and approving it for publication was Jenny Mahoney.

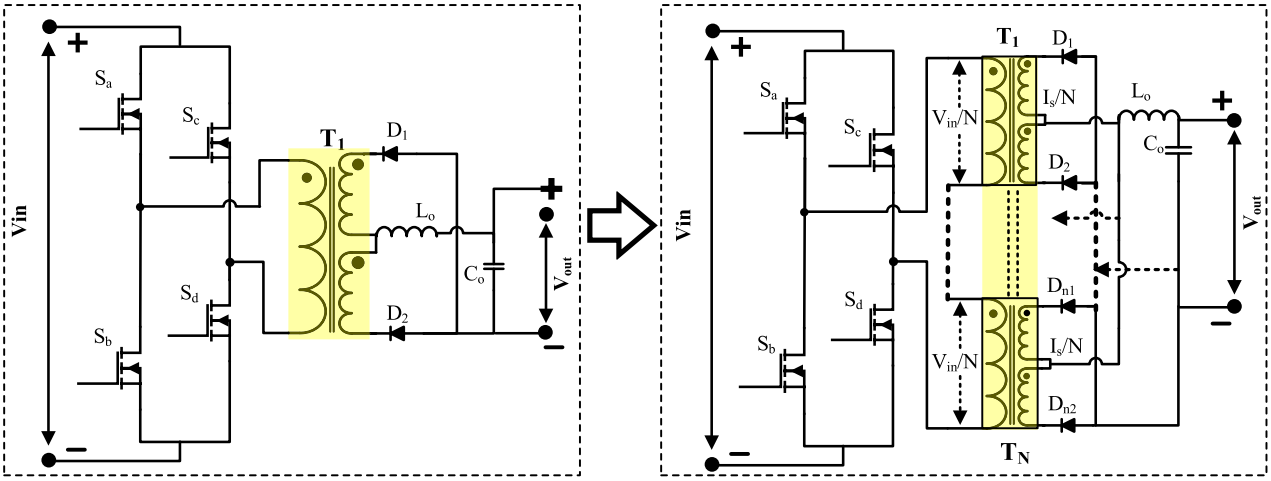

FIGURE 1. Transformation of a traditional single transformer into a number of small transformers in an example converter.

to the transformer. The decrease in the applied voltage not only improves the size and efficiency of the transformer but also eliminates the need to increase the switching frequency for improved power density.

The overall volume and weight of a power converter can be reduced by splitting a single bulky transformer into a number of small transformers. In practice, the transformer design is often based on the heating that is allowed in the transformer without overheating. The acceptable power loss can be distributed in a split transformer design as the loss per transformer reduces and the thermal path becomes much shorter. This indicates that designing the power converter with more than one transformer connected in series would make the design more compact than if there was only a single transformer. For example, when splitting a single main transformer into a series connection of N transformers, each transformer is subject to the applied voltage N times smaller than for a single transformer. The allowed power loss spreads among N low profile transformers, simplifies heat management and improves the power density. This concept is shown in Fig. 1 as an example case of a full bridge converter, where a single transformer is split into N transformers. The primary winding of N transformers is connected in series and the secondary winding is connected in parallel. The reduced input voltage to the transformers reduces the turn ratio for the given input and power application. Consequently, this helps to reduce the amount of copper in the transformer. In addition, this configuration also reduces the current stress on the secondary rectifiers by the number of transformers. For a particular application, splitting the transformer into two or four, connected in series on the primary side and parallel on the secondary side, assuming constant overall transformer loss, the parameters seen for each individual transformer change according to table 1.

A range of power converters has been discussed along with the configuration of series-connected transformers. In [5]–[12] authors discuss the phase shifted full bridge converter with more than one transformers connected in series on the primary side, and in [13]–[17] there is a discussion on LLC power converters along with the series configuration of multiple transformers. However, the discussion regarding how to split a single transformer into a number of transformers is lacking in the literature. Moreover, the configuration of series-connected transformers has not been addressed in order to achieve the goal of improved power density. Instead, the main focus on the use of more than one transformer has been to balance the output current in multi-level resonant converters; as clamper to reduce the stress on rectifiers and; to balance and reduce the input current. In [12], the focus is on eliminating the need for output filter inductor by using series-connected transformers. However, the reduction in output filter inductance reduces the range of zero voltage switching (ZVS) of the lagging leg. In [13] and [17], the series-connected transformers have been utilized for improved power density and better heat management in LLC power converters, but the methodology of splitting the design into a number of small transformers has not been discussed.

This work mainly focuses on the methodology in order to split the main single transformer into a number of small transformers. A generalized method is developed that can be easily used by replacing with the specifications for the intended power applications. The proposed work follows the

TABLE 1. Comparison of key parameters for each transformer.

# Transformers	1	2	4
Primary voltage per transformer	V_{in}	$V_{in}/2$	$V_{in}/4$
Secondary voltage	V_s	V_s	V_s
Primary current	I_p	I_p	I_p
Secondary current per transformer	I_s	$I_s/2$	$I_s/4$
Turn ratio n, n_p/n_s	n	$n/2$	$n/4$
Allowed power loss, P_{loss}	P_{loss}	$P_{loss}/2$	$P_{loss}/4$

traditional methodology of how to make a design procedure generalized and easy to implement. The resulting methodology/configuration is evaluated in an example application of an isolated dc-dc converter where the main transformer is split into a number of small transformers. The phase shifted full bridge converter is selected for the example application, and the topology is selected for its advantages over counterparts in medium and high power applications, such as zero voltage switching of all power devices and low EMI. Although the procedure is taken over for phase shifted full bridge converter, it can also be used in other applications. Different configurations of the transformers have been compared analytically to examine the losses in the main transformer. For the example application, the converter is built with a four series-connected transformer configuration and is investigated for input voltage $V_{in} = 400\ \mathrm{V_{dc}}$, output voltage $\mathrm{V}_{out} = 48\ \mathrm{V_{dc}}$ and up to the load power of 2.2 kW. The results are based on the characterization of the converter both on the prototype and on the computer simulation.

The remainder of this article is structured as follows: in the next section, the procedure of splitting the main transformer into small transformers is discussed, followed by a comparison of loss between different configurations, and finally the performance of the example application is discussed.

II. THE PROCEDURE OF DESIGNING SPLIT TRANSFORMERS

The design of a power transformer is usually based on the specification of the converter and the chosen topology. There are multiple design approaches [18]–[21] available in the literature on how to estimate the initial size of the cores of a transformer. However, there is a lack of a discussion on how to divide the estimated volume into a number of transformers. The power handling capability of a transformer depends on the type and characteristics of the core material as well as the physical geometry, i.e. area and length of the magnetic path. Furthermore, the choice of appropriate core geometry for the intended specification always needs a number of iterations throughout the design phase. The design procedure of the transformer consists of a few general considerations. Among these, there is the selection of core material, size, and form, winding space and the diameter of the wires. Each consideration requires many iterations to meet the goal of acceptable performance. The first measure is the choice of appropriate size of the transformer for the intended application.

The methods available in the literature require predetermining the core material, winding fill area, and the allowed core and copper loss. The most commonly used approaches are the evaluation of the window-area products and the measure of geometrical constant K_g. Both methods require determining the maximum flux density and value of the wire's current density in advance [22]. However, the optimum value of these factors depends on the geometry of the core [23]. This makes them less optimized, because in most applications, the maximum operating flux density is limited by the allowed core loss rather than saturation. The other limitation of these methods is that the dc copper loss is considered evenly distributed between both sections of the windings, i.e. the primary winding and the secondary winding. Moreover, copper and core loss are not accounted for together in these methods. In [24]–[30], an approach similar to the K_g method is discussed; it is called the effective core geometrical constant K_{gfe}, which accounts for both the copper loss and the core loss, providing more flexibility in optimizing the operating flux density. Therefore, this work proceeds with this approach to develop a procedure for splitting a single transformer into several transformers.

The discussion on the high-frequency effects has not been accounted for in any of the above methods. The high-frequency effects severely degrade the performance of the transformer. It is well documented [31]–[33] that the winding resistance increases with the increase in number of turns and winding layers. This work also takes into consideration the high-frequency effects in order to make the initial estimation more accurate.

A. SELECTION OF CORE SIZE

Generally, the core size is chosen in such a way that it could dissipate both copper and core loss. The total loss of the transformer can be expressed as a sum of the copper loss and the core loss,

$$P_T = P_c + P_{cu} \tag{1}$$

where P_T is the total loss of the transformer, P_c and P_{cu} are the core loss and the copper loss respectively. The core loss depends on the volume of the core, operating frequency, and peak flux density. For fixed frequency applications, the core loss P_c can be estimated using the well-known Steinmetz equation as given

$$P_c = K_{fe}(B_p)^{\beta} V_c \tag{2}$$

The parameter K_{fe} is a constant of proportionality that depends on the operational frequency, β is the material loss exponent, which for ferrite material ranges from 2.6–2.8 [18], [20]. The volume of the core V_c is the product of the core's mean magnetic path length L_m and the core's cross sectional area A_c. A cross section of a core along with the key dimension is shown in Fig. 2. The copper loss also depends on the peak operating flux density B_p and can be written as a function of flux density

$$P_{cu} = \left(\sum I_p\right)^2 R_{cu} = \left[\frac{\rho\,(V_{in}t_{on})^2\left(\sum I_p\right)^2 (MLT)}{4K_u W A_c^2 B_p^2}\right] \tag{3}$$

where $V_{in}t_{on}$ is the applied volt-second, $\sum I_p$ is the sum of all the rms currents seen by the primary winding, R_{cu} is the dc resistance of the winding, ρ is the resistivity of the copper wire, MLT is the mean length of a single turn, W, A_c, and B_p are the core window area, core cross-sectional area, and the peak operating flux density respectively. The copper fill factor K_u is the ratio of the total copper area occupied by all windings to the window area of the core, i.e. $K_u = \frac{A_{cu}}{W}$

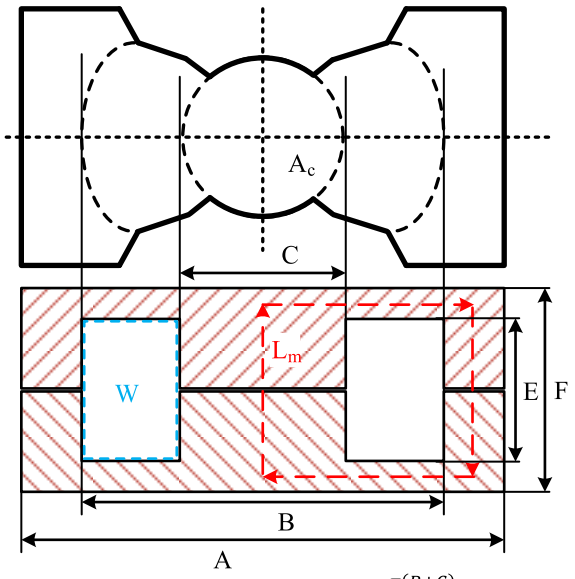

FIGURE 2. Cross-sectional view of a core, and dimensions required for the calculation of key geometrical parameters.

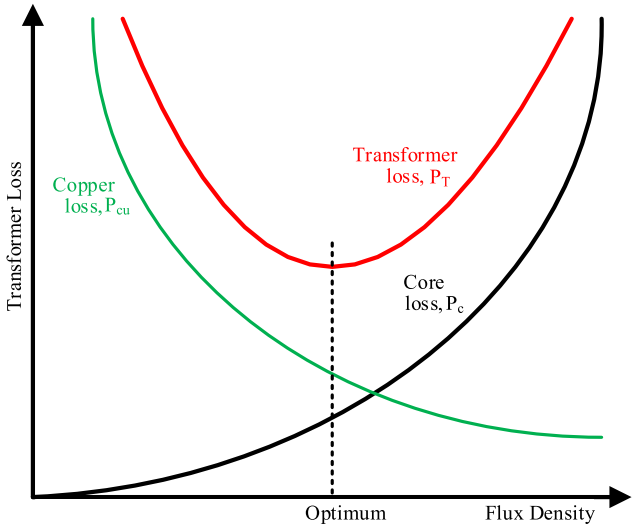

FIGURE 3. Dependency of the transformer's core, copper and total loss against the change in flux density.

As shown in equation (2) and (3), the core and copper losses both depend on the operating flux density, thus the total transformer loss depends on the chosen flux density. This dependency is shown in Fig. 3, where the optimized value of the flux density minimizes the total transformer loss [19]. At the point where the flux density is optimum, (1) can be written as

$$\frac{d\,(P_T)}{d\,(B_p)} = \frac{d\,(P_c)}{d\,(B_p)} + \frac{d\,(P_{cu})}{d\,(B_p)} = 0 \tag{4}$$

As seen in Fig. 3, since both the core loss and the copper loss, has a non-linear relationship against the flux density, the optimum flux density does not exist when the core and the copper losses are equal, rather it exists when

$$\frac{d\,(P_c)}{d\,(B_p)} = -\frac{d\,(P_{cu})}{d\,(B_p)} \tag{5}$$

Substituting (2) and (3), the derivatives of the core loss and the copper loss with respect to flux density yields

$$\frac{d\,(P_c)}{d\,(B_p)} = K_{fe}\beta(B_p)^{(\beta-1)}V_c \tag{6}$$

$$\frac{d\,(P_{cu})}{d\,(B_p)} = -2\left[\frac{\rho\,(V_{in}t_{on})^2\left(\sum I_p\right)^2(MLT)}{4K_uW\,A_c^2B_p^3}\right] \tag{7}$$

Solving (5) together with (6) and (7), for the optimum flux density

$$B_p = \left[\frac{\rho\,(V_{in}t_{on})^2\left(\sum I_p\right)^2(MLT)}{2K_uW\,A_c^3L_m\,K_{fe}\beta}\right]^{\left(\frac{1}{\beta+2}\right)} \tag{8}$$

Substituting (8) in (1) - (3) and (5), the simplified expression for the total loss results

$$P_T = \left[K_{fe}V_c\right]^{\left(\frac{2}{\beta+2}\right)}\left[\frac{\rho\,(V_{in}t_{on})^2\left(\sum I_p\right)^2(MLT)}{4K_uW\,A_c^2}\right]^{\left(\frac{\beta}{\beta+2}\right)} \times\left[\left(\frac{\beta}{2}\right)^{-\left(\frac{\beta}{\beta+2}\right)}+\left(\frac{\beta}{2}\right)^{\left(\frac{2}{\beta+2}\right)}\right] \tag{9}$$

Equation (9) is dependent on the volume and geometry of a particular core. In order to relate the core geometry with the operating conditions of the transformer, (9) is regrouped as given in (10)

$$\frac{W\,(A_c)^{\left(\frac{2(\beta-1)}{\beta}\right)}}{(MLT)\,(L_m)^{(2/\beta)}}\left[\left(\frac{\beta}{2}\right)^{-\left(\frac{\beta}{\beta+2}\right)}+\left(\frac{\beta}{2}\right)^{\left(\frac{2}{\beta+2}\right)}\right]^{-\left(\frac{\beta+2}{\beta}\right)} = \frac{\rho\,(V_{in}t_{on})^2\left(\sum I_p\right)^2K_{fe}^{(2/\beta)}}{4K_u(P_T)^{\left(\frac{\beta+2}{\beta}\right)}} \tag{10}$$

The left-hand side of (10) belongs to the parameters of the core geometry, while the right-hand side represents the specifications of the intended application as well as the parameters of the core material. As given in [20] and used in [26], the left-hand side of this equation can be termed as geometrical constant K_{gfe}, which represents the minimum value of the affective dimensions of the core for the intended application, i.e.

$$K_{gfe} = \frac{W\,(A_c)^{\left(\frac{2(\beta-1)}{\beta}\right)}}{(MLT)\,(L_m)^{(2/\beta)}} \times\left[\left(\frac{\beta}{2}\right)^{-\left(\frac{\beta}{\beta+2}\right)}+\left(\frac{\beta}{2}\right)^{\left(\frac{2}{\beta+2}\right)}\right]^{-\left(\frac{\beta+2}{\beta}\right)} \tag{11}$$

In order to design a transformer, a core with a geometrical constant that exceeds the specifications of the intended application should be selected, i.e.

$$K_{gfe} \geq \frac{\rho \left(V_{in} t_{on}\right)^2 \left(\sum I_p\right)^2 K_{fe}^{(2/\beta)}}{4K_u P_T^{\left(\frac{\beta+2}{\beta}\right)}} \tag{12}$$

In practice, the total transformer loss P_T is the loss that is allowed in the transformer. Replacing P_T as the allowed power loss P_{loss} and adding the conversion factor for meters-centimeters, (12) results

$$K_{gfe} \geq \frac{\rho \left(V_{in} t_{on}\right)^2 \left(\sum I_p\right)^2 K_{fe}^{(2/\beta)}}{4K_u P_{loss}^{\left(\frac{\beta+2}{\beta}\right)}} 10^8 \tag{13}$$

As shown in Fig.1, the applied input voltage in a split transformer approach is reduced by the number of transformers and the allowed loss is spread between the transformers. If N_T represents the total number of transformers in the configuration, then (13) can be written as

$$K_{gfe} \geq \frac{\rho \left(\frac{V_{in}}{N_T} t_{on}\right)^2 \left(\sum I_p\right)^2 K_{fe}^{(2/\beta)}}{4K_u \left(\frac{P_{loss}}{N_T}\right)^{\left(\frac{\beta+2}{\beta}\right)}} 10^8 \tag{14}$$

This equation sets the new limits for the minimum geometrical dimensions in accordance with the number of transformers in the configuration. This means that the volume of the core that is required in (13) is split between a number of transformers N_T. Therefore, the geometrical constant of each core in the configuration must satisfy (14). After selecting the core, the maximum flux density B_m and the number of primary turns can be evaluated by using (15) and (16).

$$B_m = \left[\frac{\rho \left(\frac{V_{in}}{N_T} t_{on}\right)^2 I_{prms}^2 (MLT)\, 10^8}{2K_u W L_m A_c^3 K_{fe} \beta}\right]^{\left(\frac{1}{\beta+2}\right)} \tag{15}$$

$$N_p = \frac{\left(\frac{V_{in}}{N_T} t_{on}\right) 10^4}{2B_m A_c} \tag{16}$$

The computation of converter specific parameters such as primary current I_{prms}, secondary current I_{srms} and duty cycle D depends on the topology chosen.

The optimization of the core geometry should be done for the change in wire resistivity due to the effects of high frequency. High frequency effects such as proximity loss and skin effect increase the dc resistance of the wire many times higher depending on the operational frequency and layout arrangement of the windings. This is further discussed later in this section. The increased ratio of the wire's ac resistance to the dc resistance increases the effective resistivity of the wire as

$$\rho_{eff} = \rho \left(\frac{R_{ac}}{R_{dc}}\right) \tag{17}$$

where R_{ac} and R_{dc} are the ac and dc resistance of the wire respectively. By the addition of high-frequency effects, equation (14) results

$$K_{gfe} \geq \rho \left(\frac{R_{ac}}{R_{dc}}\right) \frac{\left(\frac{V_{in}}{N_T} t_{on}\right)^2 \left(\sum I_p\right)^2 K_{fe}^{(2/\beta)}}{4K_u \left(\frac{P_{loss}}{N_T}\right)^{\left(\frac{\beta+2}{\beta}\right)}} 10^8 \tag{18}$$

In order to achieve the desired performance, after the selection of the core, wire diameter and length/structure of turns, the frequency effects should be added in the copper resistivity, then the geometrical constant of the core should satisfy (18).

B. CONSIDERATIONS OF COPPER LOSS

Copper loss is important to consider in a high-performance converter, especially for wide voltage ranges as this requires the converter to operate at low duty cycles. At a low duty cycle, the rms current increases more than the mean current and will always degrade the efficiency. After calculating the number of turns for both primary and secondary windings, the next step is selecting the correct wire/trace dimensions. The copper skin depth at the frequency of the operation should be considered before the final choice is made. Another important factor in the selection of the wire diameter is the allocation of window area to all windings. The total winding loss can be minimized with proper allocation of window area to each winding. The losses are minimal when the allocation is made relevant to the apparent power of the windings [20], [21]. In order to determine the winding geometry, it is important to evaluate the total copper loss including high-frequency effects. If the loss exceeds the allowed limit, further optimization may be required by re-iterating the design considerations.

The actual resistance of the winding is needs to be determined at the intended frequency of the operation in order to achieve the expected performance. The copper loss in combination with the core loss dissipates as heat in the form of radiation and convection. The excess heat degrades the efficiency of the transformer and consequently the performance of the system where it is installed. In the following discussion, the effective resistance of the primary and the secondary windings will be evaluated in order to estimate the copper loss.

In medium power applications, a power transformer with a hybrid structure receives more attention. In this structure, multi-strand Litz wire is used in the primary windings and the copper traces of the printed circuit board (PCB) are used as the secondary winding. This minimizes the frequency effects and makes it possible to build a low profile transformer. This work also uses the Litz wire for the primary winding and PCB traces for the secondary winding. The total copper loss is the sum of the copper loss in the primary winding and secondary winding,

$$P_{cu} = F_{Rac\_p} \left(I_{p\_rms}^2 R_{dc\_p}\right) + F_{Rac\_s} \left(I_{s\_rms}^2 R_{dc\_s}\right) \tag{19}$$

where F_{Rac} is the frequency loss factor, which is defined as $F_{Rac} = \frac{R_{ac}}{R_{dc}}$. In order to make the estimation of the copper loss more accurate, the high-frequency loss factor F_{Rac} for both the secondary winding and the primary winding needs to be determined. Therefore, for the hybrid structure of the transformer, the approximation for both winding types, i.e. copper traces and the Litz wire, are discussed separately.

The ac-dc resistance ratio mainly depends on the diameter of the wire, the number of turns and the number of winding layers. Dowell [31] derived an analytical expression for the calculation of the ac-dc resistance ratio by taking into account both the proximity and the skin effect. The Dowell expression for ac-dc resistance ratio for m-layered of a copper trace is defined as

$$F_{Rac\_s} = \Delta\left[\left\{\frac{\sinh 2\Delta + \sin 2\Delta}{\cosh 2\Delta - \cos 2\Delta}\right\} + \frac{2(m^2-1)}{3}\left\{\frac{\sinh \Delta - \sin \Delta}{\cosh \Delta + \cos \Delta}\right\}\right] \quad (20)$$

The notation Δ represents the ratio of layer height/diameter d to the skin depth, i.e. $\Delta = d/S_d$. The skin depth S_d of a conductor as a function of conductivity and frequency is defined as, $S_d = 1/\sqrt{f\sigma\pi\mu_0\mu_r}$, where σ is the conductivity of the copper, μ_0 is the magnetic permeability of air, and μ_r is the air's relative permeability. The dc resistance of the secondary winding can be calculated as

$$R_{dc\_s} = \frac{\rho N_s\,(MLT)}{A_{sec}} \quad (21)$$

where A_{sec} is the cross-sectional area of the trace of a secondary turn. Equation (20) together with (21) is used to estimate the ac-dc resistance ratio of the secondary winding.

The Dowell expression was originally derived for wide copper foil wound transformers in the one-dimensional winding structure; later it has been adapted [32]–[35] for other forms of the conductor such as round, square, rectangular and multi-strand Litz wire. The total number of turns in a layer are modeled as an effective single turn of a copper foil covering the complete window area of the core. The transformation [19]–[21] of winding with Litz wire into a single turn of copper foil is shown in Fig. 4. First, the Litz wire is replaced with a round conductor with a diameter equal to the total diameter of the Litz wire D_l. Next the round conductor is transformed into a square conductor with the same cross sectional area as the copper. The height h of the square conductor, becomes $h = \sqrt{\pi/4}D_l$. Finally, the square conductors are transformed into a layer of copper foil with a width equal to the window W of the core. During this transformation the effective cross-sectional area increases. In order to maintain the same resistivity, a porosity factor η has been introduced, which is the ratio of the copper area to the area of the effective copper foil.

For the estimation of the ac resistance of Litz wire, there are many adapted analytical models available in the literature [22], [34]–[37]. In order to apply a one-dimensional Dowell's approximation on Litz wire, each layer of strands

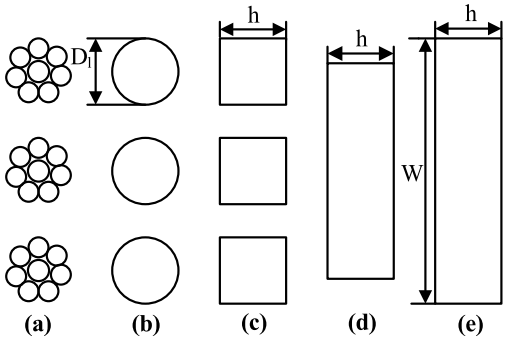

FIGURE 4. Transformation of Litz wire into a single turn of copper foil.

is first considered as a single layer of a solid wire with a thickness equal to the diameter of a strand and then it is extended to the whole winding by introducing the porosity factor. In cases where the strand diameter $d \leq S_d$, the simplified one-dimensional approach derived in the literature [35], [38], [39] and used in [22], [37] have been adopted in this work. This approach approximates the ac-dc ratio directly by modeling the physical parameters of the Litz wire such as the diameter of single strands, number of strands, bundle, and the bunch characteristics. For a Litz wire of N_l number of strands each with the diameter d, the ac-dc resistance ratio F_{Rac_p} can be approximated as

$$F_{Rac\_p} = \left[1 + \left(\frac{K_l\pi^2 N_l}{192}\right)\left\{16m_l^2 + \frac{24}{\pi^2} - 1\right\}\left(\frac{d}{2S_d}\right)^4\right] \quad (22)$$

where K_l is an effective fill factor of the Litz wire, and defined as the ratio of the effective copper area to the total area. If the total diameter of the Litz wire is D_l, then K_l can be expressed as $K_l = N_l(d/D_l)^2$. The dc resistance of the primary winding can be calculated as

$$R_{dc\_p} = \frac{4\rho N_p\,(MLT)}{\pi N_l d^2} \quad (23)$$

C. TOTAL TRANSFORMER LOSS

Once the dc resistance and the ac-dc resistance ratio F_{Rac} for both windings have become known, the copper loss is calculated by using (19). The core loss for the selected geometry of the core is calculated by using (2). The total transformer loss is then estimated by adding both the copper loss and the core loss, i.e. $P_T = P_c + P_{cu}$. If the transformer loss exceeds the allowed limits, the design needs optimization to meet the requirements of the intended application. Some of the factors that can be re-considered are the core geometry, peak flux density, and fill factor, resistance of the winding and saturation flux density of the core.

III. DESIGN EXAMPLE

In order to evaluate the performance of the proposed model, it is implemented in an example application of the dc-dc power converter. Instead of using the traditional approach of

TABLE 2. Key parameters for the design of transformers.

Input voltage (V_{in})	400 V_{dc}
Output voltage (V_o)	48 V_{dc}
Output power (P_o)	2.2 kW
Frequency (f)	260 kHz
Duty cycle (D)	0.9
PQ Core material	Magnetics Inc P-material
Allowed power loss (P_{loss})	5%
Number of transformers (N_T)	1, 2, 4
Fill factor (K_u)	0.25
Core loss exponents (β)	2.7
Core loss co-efficient (K_{fe})	7.6 W/cm^{3}Tβ
Resistivity of copper wire (ρ)	1.724x10^{-6} Ω-cm
Cross-sectional area, (A_c)	Referenced to manufacturer's data for the respective set of cores
Magnetic path length, (L_m)	
Litz Wire	d=0.1mm, N_l=200,

a single bulky transformer, a series/parallel configuration of a number of small transformers is applied in a phase shifted full bridge (PSFB) power converter. A detailed explanation of the workings of this topology is outside the scope of this article. The performance of the proposed model is first theoretically compared with the traditional design of a single transformer, after which the model is characterized in a software simulation as well as in a prototype, up to a load power of 2.2 kW.

A. TRANSFORMER DESIGN CONSIDERATIONS

The first consideration for the design of a power transformer is the evaluation of the initial size of the core according to the specification of the intended application. Next, the maximum flux density, the number of primary and secondary turns are calculated by using the parameters of the selected core. Following this, the core loss and copper loss are evaluated. Table 2 shows the specifications of the example application and other key parameters necessary to determine the core size. PQ cores are chosen in this example because of their low profile geometrical characteristics.

For the design of transformers, the iterative script of (1)-(22) along with the other converter specific equations, are written in Matlab. The parameters of the transformers, such as core size, flux density, and the number of primary/secondary turns are determined for the increased number of transformers, i.e. 1, 2 and 4. For example, in a traditional design with a single transformer, the number of transformers $N_T = 1$, equation (14) results in the minimum value of the required geometrical constant K_{gfe} as 0.0318. As shown in the table of data on PQ cores provided by the manufacturer, the smallest possible core size that fits this number is PQ-40; the given K_{gfe} for this core geometry is 0.0392. Nevertheless, if this design is built by adopting a configuration of four transformers $N_T = 4$, then the minimum required geometrical constant results in 0.0021. Looking through the manufacturer's data, it is clear that the geometry of the core's part number PQ-20

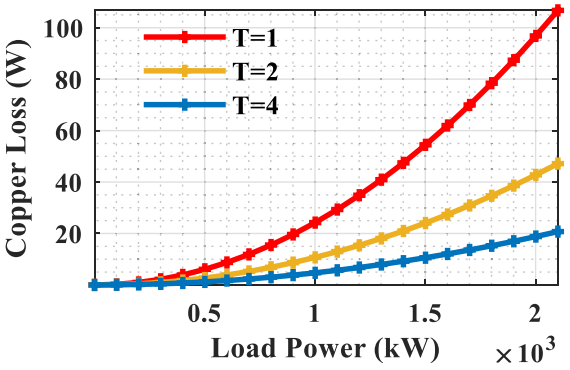

FIGURE 5. Comparison of copper loss in different transformer configurations.

meets this number. The size of PQ-20 is much smaller than the size of PQ-40. The combined weight of all four PQ-20 cores is 45% less than the weight of a single PQ-40 core. This contributes to making the power converter compact and lightweight.

Similarly, the number of primary turns and the primary to secondary turns ratio are also evaluated for the same number of transformers. There is a significant decrease in the number of turns and the turns ratio when using the configuration of four transformers. For example, in the case of design with a single transformer, the required number of primary turns and the turns ratio are 20 and 8 respectively, while the design with four transformers, this requirement is reduced to approximately 5 and 2 respectively. After the evaluation of the primary number of turns and the secondary number of turns for each configuration, the ac resistance of the primary winding and the secondary winding is estimated. Then, in order to compare the loss for each configuration, the respective core loss and the copper loss are evaluated. The core loss and the copper loss are estimated by using (2) and (19) respectively. The comparison plot of the copper loss is shown in Fig. 5, and the comparison plot for the core loss is shown in Fig. 6. As shown, both core and copper losses are minimal while in the configuration with four transformers. The increased number of turns as in the case of a single transformer $T = 1$ adds more resistive and proximity losses, and consequently more copper loss. In the configuration with four transformers, the applied volt-second is reduced by a factor four and the volume of the PQ-20 transformer is 10 times lower than a single PQ-40 transformer, which reduces the proportional core loss per transformer. As a comparison of the contribution of total transformer loss in this example, the configuration of four transformers shows better performance than the remaining two configurations. The comparison is shown in Fig. 7. At 2 kW load power the sum of the loss of all four transformers for the configuration $T = 4$ is approximately 20% less than a traditional case with a single transformer, and 10% less than the configuration with two transformers.

Therefore, the design with the configuration of four transformers is more advantageous than the design with a single bulky transformer or the design with two transformers. The

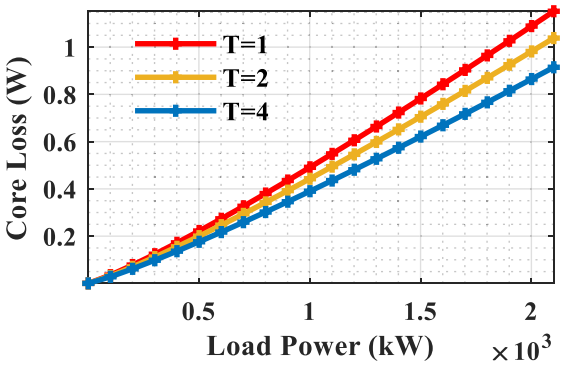

FIGURE 6. Comparison of core loss in different transformer configurations.

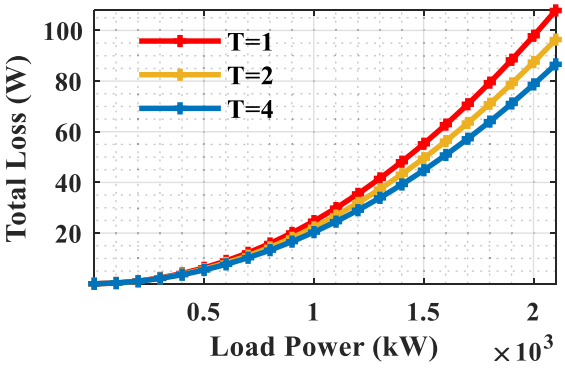

FIGURE 7. Comparison of the contribution of the total transformer loss in the example application.

reduced primary to secondary turn ratio results in improved form factor and consequently better efficiency for the transformer. The reduced number of winding turns not only decreases the copper loss but also makes it possible to design a hybrid transformer. Furthermore, by implementing the design with the four-transformer configuration, i.e. connected in series on the primary side and parallel on the secondary side, the total output current is shared by the four transformers. As a result, the current stress on the secondary side elements such as secondary winding and rectifiers is 75% less compared to the traditional approach with a single transformer. This could help improve the power density of the converter.

Since this configuration has to be implemented in the phase shifted full bridge converter, the effect of the configuration on equivalent parameters of the transformers such as magnetizing inductance, leakage inductance, and winding resistance is necessary to investigate. By connecting four transformers, series on the primary side and parallel on the secondary side, the simplified equivalent model of the configuration can be drawn as shown in Fig. 8. As seen, the magnetizing inductance of each transformer adds up to make a combined magnetizing inductance, i.e. $L_{MT} = L_{m1}+L_{m2}+L_{m3}+L_{m4}$, where L_{MT}, is the total magnetizing inductance and L_{m1} through L_{m4} are the individual magnetizing inductance of each transformer. Similarly, the individual leakage inductance of each

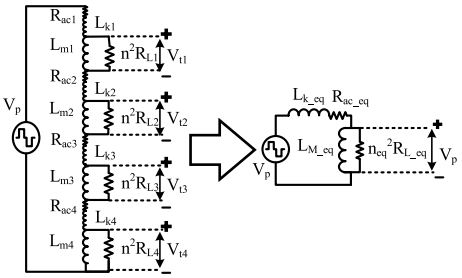

FIGURE 8. Simplified equivalent model of the configuration with four transformers.

transformer adds up as $L_{KP} = L_{kp1}+L_{kp2}+L_{kp3}+L_{kp4}$, where L_{KP} is the total leakage inductance referred to the primary side and $L_{kp1} - L_{kp4}$ are the separate leakage inductances of each transformer. This increased collective leakage inductance is helpful in soft-switched power converters such as phase shifted full bridge converters and resonant converters where the amount of leakage inductance plays a key role in determining the range of soft switching. To achieve soft switching, an extra inductor is usually required to be connected in series with the main transformer. This extra inductor is bulky and degrades the power density of the power converter; the configuration with four transformers eliminates the need for this inductor because the collective amount of leakage inductance is comparable to the inductance of this external inductor.

B. SIMULATION INVESTIGATIONS

For the computer simulation of the split transformer approach in this example application, the dc-dc converter discussed in the previous section along with the configuration of four transformers is modeled in the software LTspice. As mentioned, instead of using a single bulky transformer the required volume is split into four low profile cores. The cores selected for this example are PQ20/20 with the characteristics of 3C95 ferrite material. Fig. 9 shows the schematic diagram of the converter. As can be seen, the primary winding of each transformer is connected in series. On the secondary side, the windings are connected in parallel.

The LTspice model of the components and the operating condition for the simulation are chosen the same way as for the prototype. Wolfspeed part number CMF20120 is used as power devices S_A-S_D, and ON Semiconductor part number FSV20120 is used as rectifier devices D_1-D_8. The physical key parameters of each transformer such as magnetizing/leakage inductance and the primary/secondary winding's ac resistance are calculated and verified by using the Bode-100 impedance analyzer at the intended frequency of operation, i.e. 260 kHz. The parameters are then modeled in the simulation. In the schematic, a single inductor represents the collective primary winding leakage inductance of the entire four transformers, while on the secondary side separate inductors represent the leakage inductance of each winding. Table 3 summarizes the key components of the converter along with the physical parameters of a single transformer.

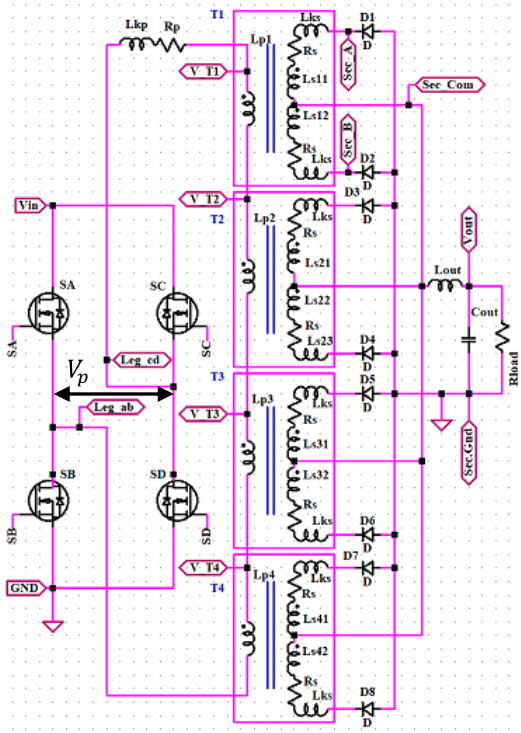

FIGURE 9. Schematic diagram of the converter with the four-transformer configuration, modeled for the simulation and the prototype characterization.

TABLE 3. Specifications/parameters of the example application.

Power devices, S_A-S_D	CMF20120
Rectifiers, D_1-D_8	FSV20120
Primary/secondary winding mutual inductance, L_p/L_s	70/20 µH
Primary/secondary leakage inductance, L_{kp}/L_{ks}	3.5/0.05 µH
Primary/secondary winding ac resistance, R_p/R_s	400/180 mΩ
Turn ratio n, N_p:N_s:N_s	4:2:2
Inductor, L_{out}	20 µH
Core cross sectional area (Ac)	0.62 cm^2
Core's magnetic path length (L_m)	3.74 cm

The switching of the primary devices is controlled by generating a typical phase shifted full bridge control drive given at gates S_A-S_D. This way, the proposed approach makes it simple to design a power converter avoiding complex control.

In PSFB converters, the legs, consisting of the power devices, are considered the leading leg and the lagging leg depending on the drive signal. Here, the leg of devices S_A-S_B is configured as the leading leg, and the leg of devices S_C-S_D as the lagging leg. Fig. 10–15 show the simulated waveforms of the converter based on the transient analysis. The operating condition for the simulation is $V_{in} = 400$ V, $V_{out} = 48$ V, $P_{out} = 2.2$ kW. The simulation running time is set to 5 ms to get stable operating points. Fig. 10 shows the waveforms of the input voltage $V(Leg_{ab}, Leg_{cd})$ to the series-connected transformers and the current I_{T1} flowing thorough the primary winding of one of the transformers. These waveforms are similar to the waveforms of the traditional PSFB converter with a single transformer. Between the power transfer intervals, there is a period where resonance occurs to charge and discharge the output capacitance of the power devices in order to prepare them for zero voltage switching. As explained in the introduction, the line voltage is divided into a number of transformers as seen in Fig 11. The differential probe $V(Leg_{ab}, Leg_{cd})$ represents the total input voltage to all four transformers, i.e. the differential voltage V_p between common points of both legs, which is equal to ±400 V. The other waveforms represent the input voltage on each transformer T_2-T_4 with respect to the common point of devices S_C and S_D i.e. leg_cd. From this, it can be seen that the voltage stress on each transformer is ±100 V instead of the full input voltage as in the case in a traditional converter with a single transformer. Fig. 12 explains the effective dc conversion ratio of the converter. The waveform $V(Leg_{ab}, Leg_{cd})$ represents the input voltage on the series-connected primary windings of all transformers, and waveforms $V(_{Sec\_A})$ and $V(_{Sec\_B})$ represent the voltage on the secondary windings of transformer T_1 with respect to the center-tapped common point. For greater legibility, here voltage $V(Leg_{ab}, Leg_{cd})$ is scaled down by four. Since the physical turn ratio of each transformer is 2:1:1 and the effective input voltage on each transformer is 100 V, each secondary winding shows a voltage swing of ±50 V. This makes the effective dc conversion ratio of the converter 8:1.

Fig. 13 shows the waveform of the current I_{Lout} flowing through the output inductor and the waveform of the current I_{Rload} flowing through the output load. As can be seen, the load current is the average of the current flowing through the output inductor. On the secondary side, the windings are connected in parallel, and the total load current will be shared between the transformers. The current in the output filter inductor reflects back towards the primary winding in accordance with the effective turn ratio of the converter. As shown in Fig. 10, the reflected current seen by the primary windings is $I_p = L_o/8 = 6.5A$. Since all four transformers are connected in series, the same amount of primary current flows through the primary winding of each transformer. Likewise, the four transformers share the total load power drawn through the converter. Fig. 14 shows a comparison of the power drawn through the load and through each transformer. Fig. 14 (bottom) shows that the average load power is approximately 2.2 kW, and the average power drawn through one of the transformers T_1 is approximately 0.55 kW. Given the combined power of the four transformers, the average of the total load power is as shown in Fig. 14 (top).

All four transformers share the total output power equally. Less power drawn through the transformers results in less heat, compared to the design with a single transformer. This means that the total heat spread among the four transformers results in better heat management. On the secondary side, four transformers in parallel share the total output current flowing through the load equally. The sum of the current flowing through each secondary winding represents the total output current. It has been mentioned earlier that the turns ratio

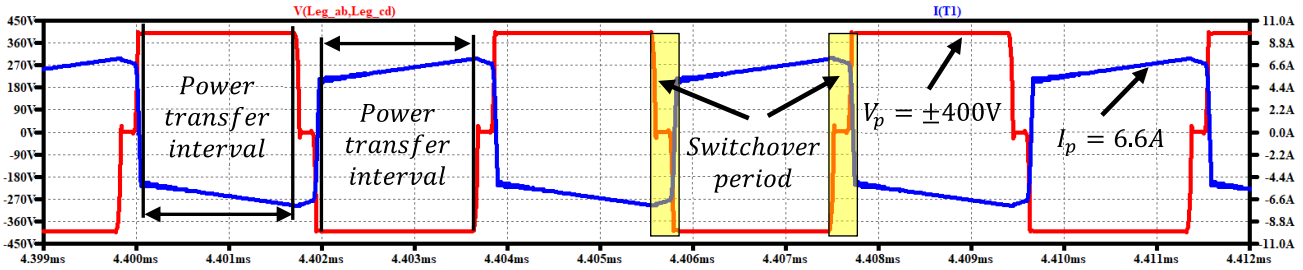

FIGURE 10. Simulated waveforms of the transformer input voltage V_p and primary current I_p.

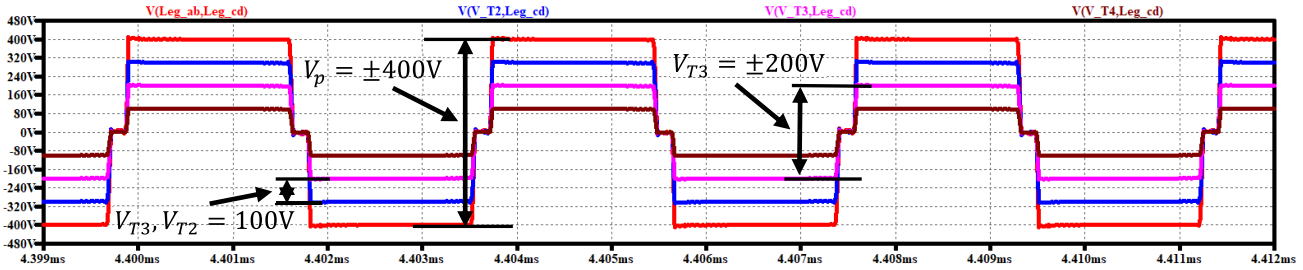

FIGURE 11. Voltage stress on transformers; input voltage is divided between four transformers, making the stress on each transformer 100V.

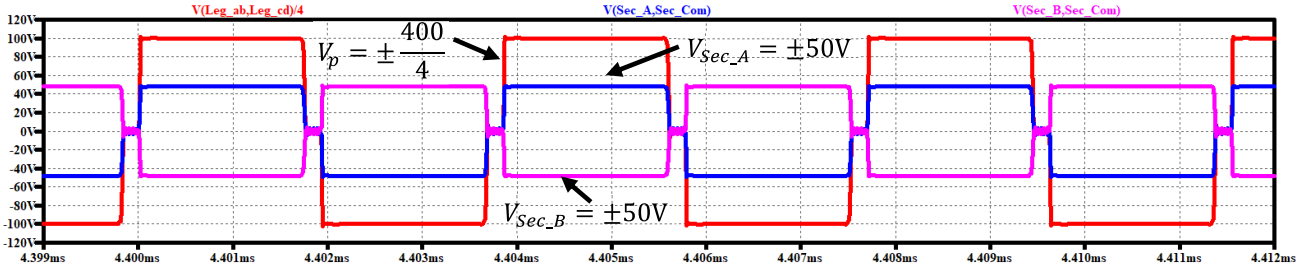

FIGURE 12. Effective dc gain of 2:1 transformers, voltage on the input of series-connected transformers and on both secondary windings of one of the transformers.

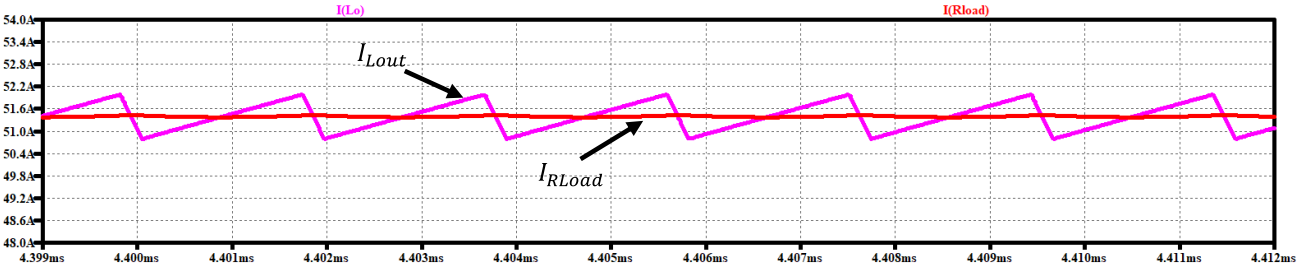

FIGURE 13. The load current equals the average of the current flowing through the output filter inductor.

decreases as the number of transformer increases, in addition to this, since four times less current is flowing through the secondary windings, the copper loss is significantly reduced compared to the traditional design. This reduced current also reduces the power rating for the secondary side elements of the converter, and hence the possibility to reduce the size of the devices.

The soft switching characteristics of all the power devices have also been observed. Fig. 15 shows the switching of all four power devices S_A-S_D. The waveforms show the gate-source voltage along with the drain-source voltage of the respective device. For better comparison, the voltage level in the waveform of the drain-source voltage is scaled down by four. As can be seen, all the devices turn ON when the

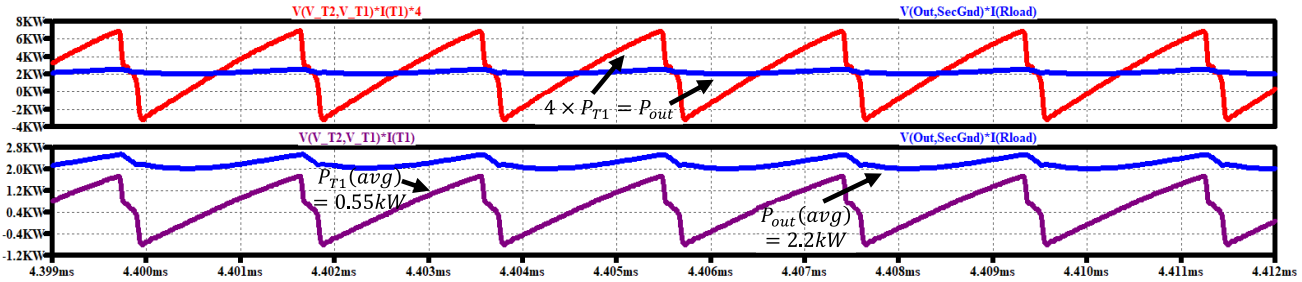

FIGURE 14. Distribution of load among four transformers, the sum of the average power drawn by each transformer is the average of the load power.

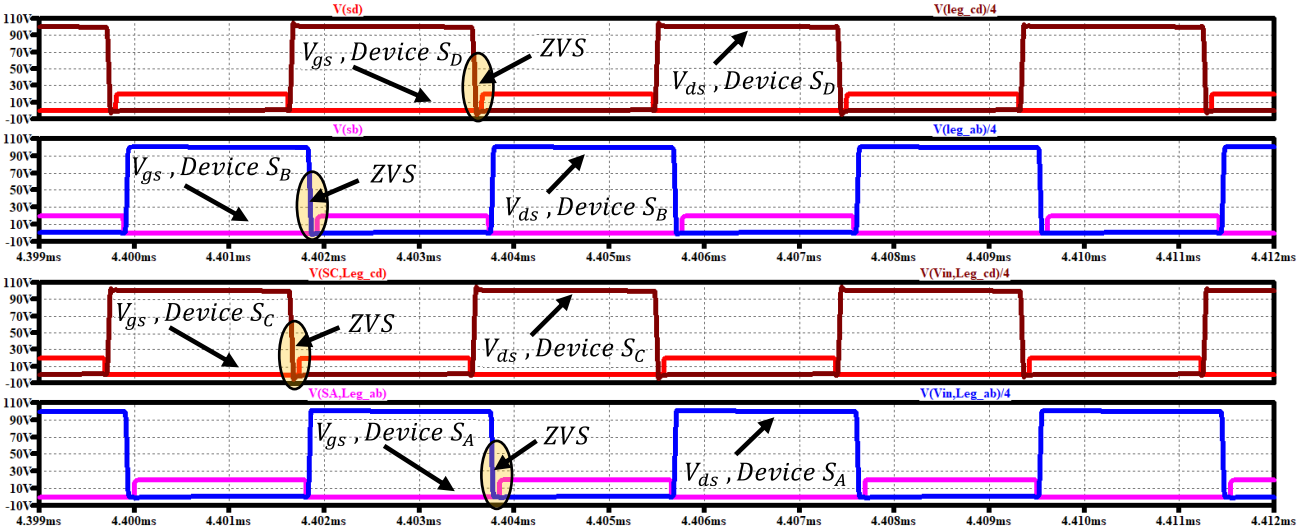

FIGURE 15. Soft switching characteristics of all four power devices at a load power of 2.2 kW, all devices observe ZVS.

drain-source voltage is at zero volts, i.e. observing zero voltage switching.

C. PROTOTYPE INVESTIGATIONS

For the validation of the proposed model in experimental work, a prototype of the converter is designed by using the same components/parameters as used in the simulation. Since the split transformer approach of four transformers reduces the number of winding turns and provides the possibility to build a hybrid transformer, the prototype is designed in such a way that the turns of the secondary winding are made on PCB with 105 μm of copper weight, and Litz wire is used for the turns of the primary winding. This shapes the final assembly into a low profile and a compact module. For better thermal management, the components are assembled on the inner side of the module, and the appropriate size and quantity of thermal vias are designed so that heat can dissipate through these vias and then to the heat sinks. Fig. 16 shows this concept. The final assembly can be placed between the appropriate size of heat sink plates to further cool down the cores and other parts.

In this example, the primary and secondary number of turns are four and two respectively. This makes the turn ratio of each transformer 2:1:1. For better power handling capabilities, two turns for each secondary winding are made on a multi-layered PCB by placing two layers in parallel and the remaining two in series. The turns of the primary winding are wound directly on the center pole of each transformer. Typical switching control for the PSFB converter is driven by using the digital signal processor. The prototype is also characterized for the isolated load power of 2.2 kW. The switching frequency is set to 260 kHz, and the converter is tested at the input voltage of 400 V. All of the key signals of the converter, e.g. switching of primary/secondary devices, voltage, and current waveforms have been investigated to ensure stable operation. The operation of the proposed converter is simple to investigate because all of the key waveforms have the same characteristics as the typical waveforms of a phase shifted full bridge converter. Fig. 17 shows the input voltage to the transformers $V(Leg_{ab}, Leg_{cd})$ and the output voltage of the converter. Channel 2 is the differential input voltage between the common points of both legs, and channel 3 is the output voltage of the converter. As can be seen, the input voltage of the transformer is $\pm$400 V, the effective dc conversion ratio of the converter is 8:1, which makes the output voltage approximately 48 V.

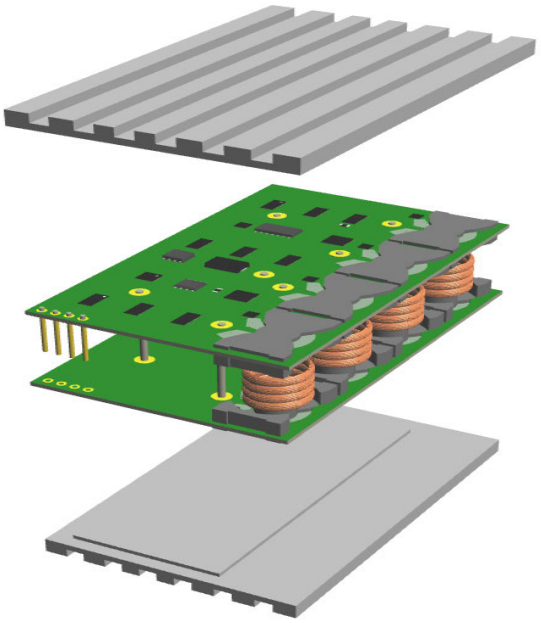

FIGURE 16. Layout plane of the converter along with the configuration of four transformers.

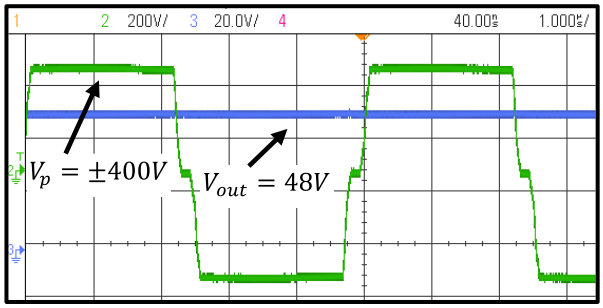

FIGURE 17. Demonstration of the dc gain of the converter, the effective gain of the converter is 8:1, Ch-2: 200 V/div, Ch-3: 20 V/div, time base: 1 μsec/div.

In a phase shifted full bridge converter, there is a leading leg and a lagging leg. The leg whose devices turn OFF first is considered the leading leg. Here the devices S_A-S_B is configured as the leading leg, and the devices S_C-S_D as the lagging leg. As discussed, by connecting the transformers in series, the individual leakage inductance of the transformers will also be added. The total leakage inductance acts as an inductor connected in series between the leading and lagging legs. This behaves exactly like an external inductor in a traditional phase shifted full bridge power converter. In order to verify this, zero voltage switching of both the leading leg and lagging leg has been investigated for the wide range of output power. For this, the drain-source voltage of the low side devices of both the legs S_B and S_D along with respective gate-source voltage have been monitored. A common issue in the phase shifted full bridge converters is that the lagging leg loses the soft switching under light load conditions because the only energy available for the commutation of the devices of this leg is the energy stored in the leakage inductance. The

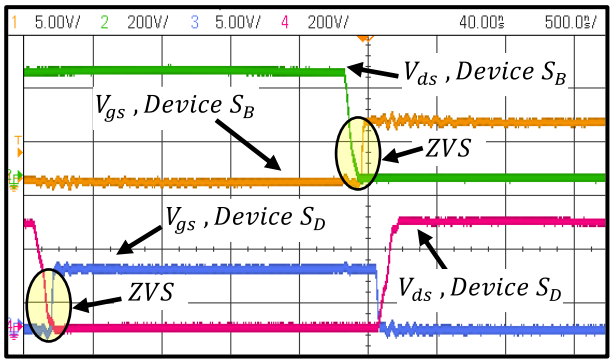

FIGURE 18. Soft switching characteristics of the leading leg and lagging leg at a load power of 1 kW, Ch-1 and Ch-3: 5V/div, Ch-2 and Ch-4: 200V/div, time base: 0.5 μsec/div.

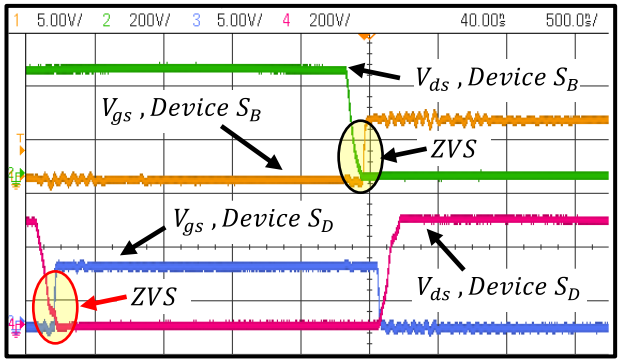

FIGURE 19. Soft switching characteristics of the leading leg and lagging leg at a load power of 0.2 kW, Ch-1 and Ch-3: 5V/div, Ch-2 and Ch-4: 200V/div, time base: 0.5 μsec/div.

converter shows good soft switching characteristics for a wide range of load power. Fig. 18 and Fig. 19 shows the switching characteristics of the devices under 50% of the rated load and 10% of the rated load respectively. As seen, at about 50% of the load, the device of both the leading leg S_B and the lagging leg S_D turns ON when the drain-source voltage is zero voltage, observing complete ZVS, at 10% of the load, the device of the lagging leg partially enters into hard switching, whereas the device of the leading leg remains soft switched. This is because only the energy stored in the leakage inductor is available for the soft switching of the lagging leg. In phase shifted full bridge converters, it is a difficult task to achieve soft switching simultaneously in both legs over the full range of the load power. Finding optimal operating conditions for both legs is necessary. The addition of extra inductance and/or implementing the adaptive control strategy can increase the range of ZVS at light load.

The temperature profile of all sections of the converter is monitored by using the Fluke Ti9 infrared camera and the inside of the module is recorded using thermocouple probes. The heat from rectifiers dissipates through vias on the aluminum plate of thickness 3 mm. The heat from the cores of the transformers dissipates directly into the air. All of the measurements have been performed at room temperature. Fig. 20 shows the temperature profile of the converter operating

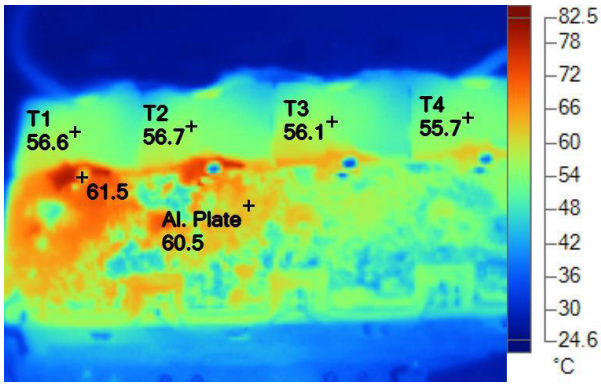

FIGURE 20. Temperature profile of the transformers; all cores show the same temperature, the hottest spot is the termination point of the secondary windings.

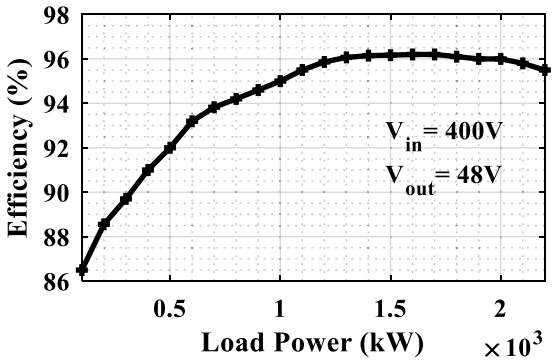

FIGURE 21. Efficiency of the converter for the variation of the load power 0.1 kW- 2.2 kW.

at a load power of 2.2 kW. The thermocouples report a maximum inside temperature of approximately 45 °C.

The surface temperature of the key elements has been marked by using PC software. As can be seen, the surface temperature of the cores of all four transformers labelled T_1-T_4 is the same, which is approximately 56 °C. This indicates that an equal amount of flux and current flows through the series combination of four transformers, and all transformers share the total load power. The temperature of the aluminum plate rises to about 60 °C. The whole assembly can be further cooled down by the use of appropriate thermal management. Fig. 20 shows that the maximum recorded temperature is the termination point of the secondary windings. The full output current flows through these points. The temperature rise at this common point is approximately 61 °C. The heat spreads out to the adjacent components as seen in cores and surrounding areas. This can be rectified by improving the layout plan and enhancing the current carrying capacity of these termination points.

In addition to the improved power density, the efficiency of the converter also plays a major role in the development of a power system. The efficiency of the converter along with the proposed configuration of transformers has been measured over the full range of the load power. Fig. 21 demonstrates the performance of the converter for the variation in load power. Here the load varies from 0.1 kW to 2.2 kW. The recorded peak efficiency is approximately 96%, which is comparable with the counterparts working at this frequency and input/load level. This can further be improved by the use of low loss devices. As discussed, the contribution of all four transformers in the total losses is 3%, and this contribution will be more than 5% if the converter had been built using the traditional approach with a single transformer.

IV. CONCLUSION

A method to split a single bulky transformer into a number of small transformers is presented. The method is verified both analytically and experimentally in an example application with a phase shifted full bridge converter. As comparison with the traditional design, the suggested design reduces the weight and volume of the converter by ∼45%, which results in improved power density. It is observed that the design with split transformer method does not affect the traditional characteristics of the converter that also simplifies the implementation. Furthermore, the design of power converters by splitting the main transformer into a number of transformers not only makes the converter low profile but also reduces the stress on the transformer and rectifiers. The reduced core loss and copper loss minimizes the proportional losses in transformers. By spreading the losses between a number of transformers heat management is simplified. A parallel configuration on the secondary section also decreases the required current rating of the rectifiers, inductors, and capacitors, and improves the power density. The prototype investigations are consistent with the analytical and simulation results. The reported efficiency is also comparable with the converter of this class. Based on the investigations, it can be concluded that the presented split transformer design method can help to improve the power density of converters in order to meet present and future requirements of the industry.

REFERENCES

[1] B. K. Bose, "Power electronics, smart grid, and renewable energy systems," *Proc. IEEE*, vol. 105, no. 11, pp. 2011–2018, Nov. 2017.

[2] K. A. Kim, Y.-C. Liu, M.-C. Chen, and H.-J. Chiu, "Opening the box: Survey of high power density inverter techniques from the little box challenge," *CPSS Trans. Power Electron. Appl.*, vol. 2, no. 2, pp. 131–139, Jun. 2017.

[3] X. Li, S. Dusmez, U. R. Prasanna, B. Akin, and K. Rajashekara, "A new SVPWM modulated input switched multilevel converter for grid-connected PV energy generation systems," *IEEE J. Emerg. Sel. Topics Power Electron.*, vol. 2, no. 4, pp. 920–930, Dec. 2014.

[4] S. Waffler and J. W. Kolar, "A novel low-loss modulation strategy for high-power bidirectional buck + boost converters," *IEEE Trans. Power Electron.*, vol. 24, no. 6, pp. 1589–1599, Jun. 2009.

[5] B. Gu, J.-S. Lai, N. Kees, and C. Zheng, "Hybrid-switching full-bridge DC–DC converter with minimal voltage stress of bridge rectifier, reduced circulating losses, and filter requirement for electric vehicle battery chargers," *IEEE Trans. Power Electron.*, vol. 28, no. 3, pp. 1132–1144, Mar. 2013.

[6] G. Ning, W. Chen, L. Shu, and X. Qu, "A hybrid ZVZCS dual-transformer-based full-bridge converter operating in DCM for MVDC grids," *IEEE Trans. Power Electron.*, vol. 32, no. 7, pp. 5162–5170, Jul. 2017.

[7] C.-H. Chien, B.-R. Lin, and Y.-H. Wang, "Analysis of a novel resonant converter with series connected transformers," *IET Power Electron.*, vol. 6, no. 3, pp. 611–623, Mar. 2013.

[8] B.-R. Lin and C.-H. Chao, "Analysis of an interleaved three-level ZVS converter with series-connected transformers," *IEEE Trans. Power Electron.*, vol. 28, no. 7, pp. 3088–3099, Jul. 2013.
[9] X. Yu, M. R. Starke, L. M. Tolbert, and B. Ozpineci, "Fuel cell power conditioning for electric power applications: A summary," *IET Electr. Power Appl.*, vol. 1, no. 5, pp. 643–656, 2007.
[10] B.-R. Lin, H.-K. Chiang, C.-C. Chen, and F.-Y. Hsieh, "Soft switching converter with series-connected transformers," in *Proc. TENCON IEEE Region 10 Conf.*, Nov. 2006, pp. 1–4.
[11] H.-K. Yoon, S.-K. Han, E.-S. Choi, G.-W. Moon, and M.-J. Youn, "Zero-voltage switching and soft-commutating two-transformer full-bridge PWM converter using the voltage-ripple," *IEEE Trans. Ind. Electron.*, vol. 55, no. 3, pp. 1478–1488, Mar. 2008.
[12] R. Ayyanar and N. Mohan, "Novel soft-switching DC-DC converter with full ZVS-range and reduced filter requirement—Part II: Constant-input, variable-output applications," *IEEE Trans. Power Electron.*, vol. 16, no. 2, pp. 193–200, Mar. 2001.
[13] C. Fei, F. C. Lee, and Q. Li, "High-efficiency high-power-density LLC converter with an integrated planar matrix transformer for high-output current applications," *IEEE Trans. Ind. Electron.*, vol. 64, no. 11, pp. 9072–9082, Nov. 2017.
[14] B.-R. Lin and J.-Y. Dong, "ZVS resonant converter with parallel–series transformer connection," *IEEE Trans. Ind. Electron.*, vol. 58, no. 7, pp. 2972–2979, Jul. 2011.
[15] M. Yu, D. Sha, Z. Guo, and X. Liao, "Hybrid PS full bridge and LLC half bridge DC-DC converter for low-voltage and high-current output applications," in *Proc. Conf. IEEE Appl. Power Electron. Conf. Expo. (APEC)*, Mar. 2014, pp. 1088–1094.
[16] I. Demirel and B. Erkmen, "A very low-profile dual output LLC resonant converter for LCD/LED TV applications," *IEEE Trans. Power Electron.*, vol. 29, no. 7, pp. 3514–3524, Jul. 2014.
[17] Y. Shen, W. Zhao, Z. Chen, and C. Cai, "Full-bridge LLC resonant converter with series-parallel connected transformers for electric vehicle on-board charger," *IEEE Access*, vol. 6, pp. 13490–13500, 2018.
[18] W. T. McLyman and C. W. M. T. Mclyman, "Power transformer design," in *Transformer Inductor Design Handbook*, 4th ed. Boca Raton, FL, USA: CRC Press, 2011, pp. 30–60 and 100–500.
[19] W. G. Hurley and W. H. Wölfle, *Transformers and Inductors for Power Electronics*. Hoboken, NJ, USA: Wiley, 2013.
[20] R. W. Erickson and D. Maksimović, *Fundamentals of Power Electronics*. Boston, MA, USA: Springer, 2001.
[21] M. Kazimierczuk, *High-Frequency Magnetic Components*. Chichester, U.K.: Wiley, 2013.
[22] E. L. Barrios, A. Ursua, L. Marroyo, and P. Sanchis, "Analytical design methodology for Litz-Wired high-frequency power transformers," *IEEE Trans. Ind. Electron.*, vol. 62, no. 4, pp. 2103–2113, Apr. 2015.
[23] F. Forest, E. Laboure, T. Meynard, and M. Arab, "Analytic design method based on homothetic shape of magnetic cores for high-frequency transformers," *IEEE Trans. Power Electron.*, vol. 22, no. 5, pp. 2070–2080, Sep. 2007.
[24] L. Hsiu and A. F. Witsulski, "A geometrical core constant approach to integrated magnetics design," in *Proc. 4th IEEE Int. Power Electron. Congr. Tech. (CIEP)*, Oct. 1995, pp. 108–116.
[25] C. W. T. McLyman, "Designing a continuous current buck-boost converter using the core geometry," in *Proc. Elect. Insul. Conf. Elect. Manuf. Expo*, 2005, pp. 329–336.
[26] S. Barg, K. Ammous, H. Mejbri, A. Alahdal, and A. Ammous, "Optimum design approach of high frequency transformer," in *Proc. Asia–Pacific Int. Symp. Electromagn. Compat. (APEMC)*, May 2016, pp. 553–556.
[27] M. Frivaldsky, P. Spanik, P. Drgona, and O. Hock, "Influence of transformer core geometry on the qualitative indexes of front-end converters," in *Proc. ELEKTRO*, May 2014, pp. 170–175.
[28] R. Petkov, "Optimum design of a high-power, high-frequency transformer," *IEEE Trans. Power Electron.*, vol. 11, no. 1, pp. 33–42, Jan. 1996.
[29] W. G. Hurley, W. H. Wolfle, and J. G. Breslin, "Optimized transformer design: Inclusive of high-frequency effects," *IEEE Trans. Power Electron.*, vol. 13, no. 4, pp. 651–659, Jul. 1998.
[30] R. A. Jabr, "Application of geometric programming to transformer design," *IEEE Trans. Magn.*, vol. 41, no. 11, pp. 4261–4269, Nov. 2005.
[31] P. L. Dowell, "Effects of eddy currents in transformer windings," *Proc. Inst. Elect. Eng.*, vol. 113, no. 8, pp. 1387–1394, 1966.
[32] J. A. Ferreira, "Improved analytical modeling of conductive losses in magnetic components," *IEEE Trans. Power Electron.*, vol. 9, no. 1, pp. 127–131, Jan. 1994.
[33] A. Reatti and M. K. Kazimierczuk, "Comparison of various methods for calculating the AC resistance of inductors," *IEEE Trans. Magn.*, vol. 38, no. 3, pp. 1512–1518, May 2002.
[34] W. G. Hurley, E. Gath, and J. G. Breslin, "Optimizing the AC resistance of multilayer transformer windings with arbitrary current waveforms," *IEEE Trans. Power Electron.*, vol. 15, no. 2, pp. 369–376, Mar. 2000.
[35] F. Tourkhani and P. Viarouge, "Accurate analytical model of winding losses in round Litz wire windings," *IEEE Trans. Magn.*, vol. 37, no. 1, pp. 538–543, 2001.
[36] R. P. Wojda and M. K. Kazimierczuk, "Winding resistance and power loss of inductors with Litz and solid-round wires," *IEEE Trans. Ind. Appl.*, vol. 54, no. 4, pp. 3548–3557, Jul. 2018.
[37] A. Garcia-Bediaga, I. Villar, A. Rujas, L. Mir, and A. Rufer, "Multiobjective optimization of medium-frequency transformers for isolated soft-switching converters using a genetic algorithm," *IEEE Trans. Power Electron.*, vol. 32, no. 4, pp. 2995–3006, Apr. 2017.
[38] C. R. Sullivan, "Optimal choice for number of strands in a Litz-Wire transformer winding," *IEEE Trans. Power Electron.*, vol. 14, no. 2, pp. 283–291, Mar. 1999.
[39] R. P. Wojda and M. K. Kazimierczuk, "Winding resistance of Litz-Wire and multi-strand inductors," *IET Power Electron.*, vol. 5, no. 2, p. 257, 2012.

M. ABU BAKAR received the M.S. degree in the field of power engineering from Mid Sweden University, Sweden, in 2012, where he is currently pursuing the Ph.D. degree in power engineering. He has years of industrial experience designing a customized solution related to electrical and electronics engineering. His research interests include power electronics and analog and digital electronics.

M. FARHAN ALAM received the B.S. degree in electronics from Air University Islamabad, Pakistan, in 2007, and the M.S. degree in electronics from Mid Sweden University, Sundsvall, in 2012.

From 2012 to 2016, he worked as a Design Engineer at SEPS AB Sundsvall Sweden, where time he worked with high-frequency GaN power converters and designing electronic marker locator. Since 2016, he has been a Research Assistant with the Power Electronics Group, Mid Sweden University. His research interests include the development of a microcontroller system designing PCB for power converters testing and characterization of power converters.

KENT BERTILSSON received the M.Sc. degree in electronics from Mid Sweden University, Sundsvall, Sweden, in 1999, and the Ph.D. degree in the field of device design and optimization of silicon carbide devices from the Royal Institute of Technology, Stockholm, Sweden, in 2005. Since 2005, he is leading the research in power electronics at Mid Sweden University, where he is currently a Full Professor. In 2009, he co-founded SEPS Technologies AB, Sundsvall, where he is also the CEO. He has authored or coauthored more than 60 articles in international journals and conferences in the fields of semiconductor device simulations, silicon carbide devices, detectors, and power electronics.